'92 KACC 1992. 10. 19~21

Dextrous Sensor Hand for the Intelligent Assisting System — IAS

Hideki HASHIMOTO and Martin BUSS

Institute of Industrial Science, University of Tokyo
7-22-1 Roppongi, Minato-ku, Tokyo 106, Japan
Tel +81-3-3402-6231 Ext 2359/2360 Fax +81-3-3423-1484
E-mail: martin@ics.iis.u-tokyo.ac.jp

Abstract : *The goal of the proposed Intelligent Assisting System - IAS is to assist human operators in an intelligent way, while leaving decision and goal planning instances for the human. To realize the IAS the very important issue of manipulation skill identification and analysis has to be solved, which then is stored in a Skill Data Base. Using this data base the IAS is able to perform complex manipulations on the motion control level and to assist the human operator flexibly. We propose a model for manipulation skill based on the dynamics of the grip transformation matrix, which describes the dynamic transformation between object space and finger joint space. Interaction with a virtual world simulator allows the calculation and feedback of appropriate forces through controlled actuators of the sensor glove with 10 degrees-of-freedom. To solve the sensor glove calibration problem, we learn the nonlinear calibration mapping by an artificial neural network (ANN). In this paper we also describe the experimental system setup of the skill acquisition and transfer system as a first approach to the IAS. Some simple manipulation examples and simulation results show the feasibility of the proposed manipulation skill model.*

Keywords: Intelligent Manipulation, Dextrous Manipulation, Grip Transform, Virtual Reality, Skilled Manipulation, Skill Analysis, Human Skill Transfer.

1 Introduction

We have proposed the Intelligent Assisting System - IAS as a new forthcoming research topic [2][3]. Using this system we are approaching the identification and analysis of human manipulation skills. Humans can effectively manipulate a great variety of objects, without thinking about it consciously, and handle objects despite of environment uncertainties in an amazingly adaptive and robust way.

Once manipulation skill can be identified and modeled, it can be learned leading to a Skill Data Base. Using this data base the IAS will be able to perform rather complex manipulations on the motion control level and the operator can do the task by only giving the goal in a preferably abstract form. The actual manipulation is then automatically performed by the IAS, which consults the operator only in unknown situations, i.e. environment states which are unknown in the skill data base. Through repeated interaction with the operator the manipulation skills in the data base can be increased on-line and the abilities of the IAS therewith increase.

Section 2 describes the system structure of the proposed IAS, with the subsections: functional description (2.1), virtual world simulator (2.2), sensor glove (2.3) and calibration (2.4). Section 3 gives a theoretical model for manipulative skill based on the grip transform first proposed by Salisbury [8] and the concept of internal grasp forces further developed by Kerr and Roth [5]. We will show in an example in section 3.2 that the dynamic behavior of this transformation matrix can be interpreted as the essence of the performed manipulation skill. Section 3.3 derives a control algorithm to realize the acquired skill using a control law in the joint actuator space of the skill executing robotic hand. Finally some experimental and simulation results are shown in section 4 followed by conclusions in section 5.

2 Skill Acquisition System

2.1 Functional Description

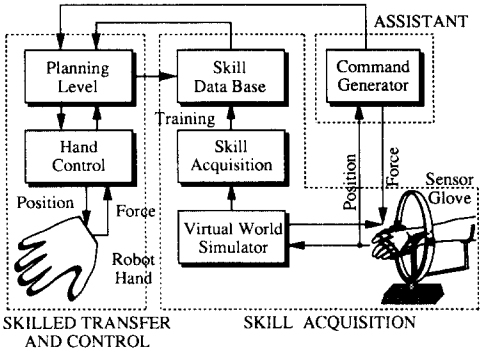

Figure 1: System Structure of the IAS.

This section describes the system structure of the skill acquisition and transfer system as a first approach to the IAS, where three signal flows can be identified (Fig. 1).

Flow 1—Skill Acquisition: A sensor glove is attached to the hand of the human operator for interaction with objects in a virtual reality. The operator gets a

feedback of the generated forces, and can so feel physically present in the virtual world. Analyzing the available data of joint torques and positions, essential parameters for the model of the performed manipulation skill can be derived, which are stored in the skill data base.

Flow 2—Skill Transfer: The acquired skill now available in the skill data base is used for intelligent control of a robotic hand. Since only essential parameters are stored in the data base, the robot hand not necessarily needs to have the same structure as the sensor glove used for skill acquisition.

Flow 3—Assisting Manipulation: In this mode the IAS performs as an assistant to the human operator. The *assistant* function block (see Fig. 1) identifies and anticipates the action the human operator wants to perform, and if the necessary skill has been stored in the skill data base before, it is applied. In case of unknown tasks, the assistant automatically switches in acquisition mode, learning new manipulation skills on-line.

2.2 Virtual World Simulator

The experimental system for skill acquisition as described above, has three main functional blocks (see Fig. 2):

(a) motion controllers for the sensor glove,

(b) calculation of forces acting on objects and the hand in the virtual world and

(c) graphics animation block as an easy-to-understand man-machine interface.

The position sensor signals of the sensor glove give information about the joint angles of the operator's hand, which are fed to both, the graphics animation block and the solid state model. New object positions due to force interactions are calculated and then fed also to the graphics animation module. Calculating the joint torques for a feedback to the sensor glove realizes a force-display.

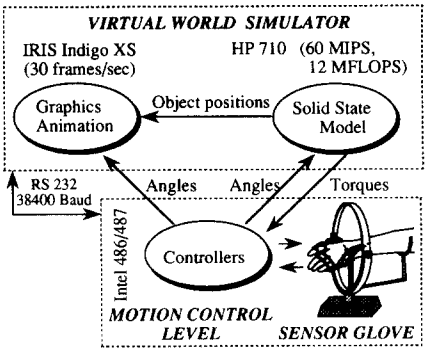

Figure 2: Experimental System Structure.

2.3 Sensor Glove Hardware

The sensor glove attached to the hand of the human operator has 10 degrees of freedom. Figure 4 shows a schematic of the sensor glove hardware structure and the joint angles of the human hand which can be measured. There are 3 degrees-of-freedom for the wrist, 3 for the index finger, 2 for the thumb and 2 for the rest of the fingers. Figure 3 shows a photo of the sensor glove hardware.

Figure 3: Photo of the Experimental System.

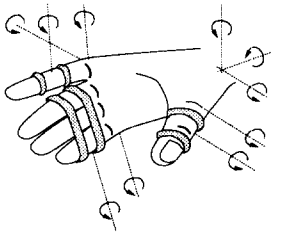

Figure 4: Schematic of Sensor Glove Structure.

2.4 Sensor Glove Calibration

Generally the structure of a sensor glove cannot be made completely identical with the kinematic hand model to which the glove inputs its sensory signals. As shown in Fig. 4 it is obvious that the two position sensor angles ψ_1, ψ_2 for the index finger coming from the glove have no simple relationship to the three angles $\theta_1, \theta_2, \theta_3$ used in the kinematic model of the human hand. The mapping between the vectors Ψ and Θ is a complex nonlinear mapping, which can be described as

$$\Theta = f(\Psi) \tag{1}$$

where $\Psi = [\psi_1 \ \ldots \ \psi_m]^T$ is the vector of sensor readings and $\Theta = [\theta_1 \ \ldots \ \theta_n]^T$ is the vector of desired joint angles of the kinematic finger model. If several people want to use the sensor glove, a different mapping function $f(\Psi)$ must be found for every person, because of different hand sizes. This mapping is learned by a standard artificial neural network (ANN) with three layers (2 inputs, 10 nodes in the hidden layer and 3 outputs). The advantage of using an ANN for the mapping also is, that for a different person operating the sensor glove a different set of weight matrices for the ANNs can be used.

3 Manipulation Skill Model

Based on the grip transformation matrix, the manipulation skill model describes the dynamic transformation between the generalized force vector acting on the object and the contact wrenches which realize these forces. We regard the dynamic behavior of the grip transform as the essence of the performed manipulation skill.

Manipulative skill can be defined as the dynamics of the

generalized external force $\boldsymbol{f}_{ext}(t)$ acting on the object. To manipulate the object in a goal-oriented way the external force vector $\boldsymbol{f}_{ext}(t)$ has to be controlled along a desired trajectory, i.e. magnitude and direction of $\boldsymbol{f}_{ext}(t)$ vary with time while moving the object on the desired trajectory. Usually $\boldsymbol{f}_{ext}(t)$ is applied by multiple contacts from fingers of a hand, where contact conditions and actuating degrees of freedom are to be coordinated in an appropriate way. We formulate the following proposition:

Proposition 1 *The time-dependent behaviour of the grip transform matrix $\boldsymbol{G}(t)$ is regarded as low level manipulative skill.*

The following section reviews the concept of force balance of the grasped object for arbitrarily applied grasp wrenches, the idea of internal forces and the definition of the grip transform $\boldsymbol{G}(t)$. Section 3.2 shows a simple manipulative skill example, illustrating Proposition 1 and in section 3.3 a control algorithm is derived which realizes a task given by object and internal grasp force trajectories. In the following all matrices and vectors used are generally time-dependent and often this is not written explicitly in the equations for simplicity.

3.1 Grip Transform

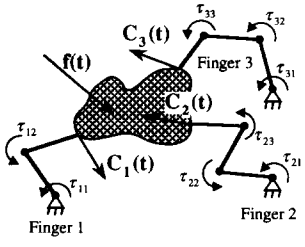

Figure 5: Object in Stable Grasp.

If an object is grasped by m fingers (see Fig. 5), contact forces and moments (wrenches) must be balanced to the external force

$$\boldsymbol{f}_{ext} = \begin{bmatrix} f_x & f_y & f_z & m_x & m_y & m_z \end{bmatrix}^T = \begin{bmatrix} \boldsymbol{f} \\ \boldsymbol{m} \end{bmatrix} \quad (2)$$

where $\boldsymbol{f}_{ext} \in \mathcal{R}^6$ is the generalized force vector. If the vector $\boldsymbol{c} \in \mathcal{R}^n$ contains the finger contact wrench intensities, the force balance can be written as

$$\boldsymbol{f}_{ext} = \boldsymbol{W}\boldsymbol{c} \quad (3)$$

where the matrix $\boldsymbol{W} \in \mathcal{R}^{6\times n}$ contains the n contact wrench directions in its columns. For the following we always assume $rank(\boldsymbol{W}) = 6$.

For a given $\boldsymbol{f}_{ext}$ there usually is no unique solution for $\boldsymbol{c}$ of Equation (3), which can be split into two vectors, the particular solution $\boldsymbol{c}_p$ and the homogenous solution $\boldsymbol{c}_h$ such that

$$\boldsymbol{c} = \boldsymbol{c}_p + \boldsymbol{c}_h \ , \quad (4)$$

where $\boldsymbol{c}_p$ is orthogonal to $\boldsymbol{c}_h$ and $\boldsymbol{c}_h \subset null(\boldsymbol{W})$ corresponding to the internal grasp forces. $\boldsymbol{c}_p$ can be calculated using the right generalized inverse of $\boldsymbol{W}$ as

$$\boldsymbol{c}_p = \boldsymbol{W}^+ \boldsymbol{f}_{ext} \ , \quad (5)$$

where $\boldsymbol{W}^+ = \boldsymbol{W}^T[\boldsymbol{W}\boldsymbol{W}^T]^{-1}$. Let us define the matrix $\boldsymbol{N} \in \mathcal{R}^{n\times(n-6)}$ containing the orthonormal basis vectors $\boldsymbol{c}_{i,h}$ in its columns, which are spanning the $(n-6)$-dimensional null space of $\boldsymbol{W}$ (i.e. $\boldsymbol{N}^T\boldsymbol{N} = \boldsymbol{I}_{n-6}$, where $\boldsymbol{I}_n \in \mathcal{R}^{n\times n}$ denotes the unity matrix) as

$$\boldsymbol{N} = \begin{bmatrix} \boldsymbol{c}_{1,h} & \boldsymbol{c}_{2,h} & \dots & \boldsymbol{c}_{n-6,h} \end{bmatrix}. \quad (6)$$

Using Equation (6) we can write $\boldsymbol{c}_h$ in terms of internal grasp forces $\boldsymbol{f}_{int} \in \mathcal{R}^{n-6}$ as

$$\boldsymbol{c}_h = \boldsymbol{N}\boldsymbol{f}_{int} \ , \quad (7)$$

where the magnitudes of the internal grasp forces are then the elements of $\boldsymbol{f}_{int}$. A method for optimizing the internal grasp forces including friction and joint torque limit constraints has been proposed by Kerr and Roth in [5].

The grip transform matrix $\boldsymbol{G}$ is defined by augmenting the matrix $\boldsymbol{W}$ of Equation (3) with the matrix $\boldsymbol{N}$ defined in Equation (6) as

$$[\boldsymbol{G}^T]^{-1} = \begin{bmatrix} \boldsymbol{W} \\ --- \\ \boldsymbol{N}^T \end{bmatrix}. \quad (8)$$

This matrix will be square, and assuming that the $(n-6)$ null space basis vectors $\boldsymbol{c}_{i,h}$ are linearly independent, $[\boldsymbol{G}^T]^{-1}$ will be invertible. Let us augment the external force $\boldsymbol{f}_{ext}$ with the internal forces $\boldsymbol{f}_{int}$ into one generalized force vector $\boldsymbol{\mathcal{F}} \in \mathcal{R}^n$ as

$$\boldsymbol{\mathcal{F}} = \begin{bmatrix} \boldsymbol{f}_{ext} \\ \boldsymbol{f}_{int} \end{bmatrix}. \quad (9)$$

Now we can write the relation between external net wrench $\boldsymbol{\mathcal{F}}$ and the n contact wrenches as

$$\boldsymbol{\mathcal{F}} = (\boldsymbol{G}^T)^{-1}\boldsymbol{c} = \begin{bmatrix} \boldsymbol{W} \\ \boldsymbol{N}^T \end{bmatrix} \boldsymbol{c} \quad (10)$$

$$\boldsymbol{c} = \boldsymbol{G}^T\boldsymbol{\mathcal{F}} = \begin{bmatrix} \boldsymbol{W}^+ & \boldsymbol{N} \end{bmatrix} \boldsymbol{\mathcal{F}} . \quad (11)$$

Using energy conservation principles we can derive the relation between the object external and internal velocities $\boldsymbol{v}_{ext}, \boldsymbol{v}_{int}$ and the twist intensities $\boldsymbol{d}$ (motion along the axes of the corresponding contact wrench) as

$$\boldsymbol{d} = \boldsymbol{G}^{-1}\boldsymbol{\mathcal{V}} = \begin{bmatrix} \boldsymbol{W}^T & \boldsymbol{N} \end{bmatrix} \boldsymbol{\mathcal{V}} \quad (12)$$

$$\boldsymbol{\mathcal{V}} = \boldsymbol{G}\,\boldsymbol{d} = \begin{bmatrix} [\boldsymbol{W}^T]^+ \\ \boldsymbol{N}^T \end{bmatrix} \boldsymbol{d} , \quad (13)$$

where

$$\boldsymbol{\mathcal{V}} = \begin{bmatrix} \boldsymbol{v}_{ext} \\ \boldsymbol{v}_{int} \end{bmatrix} \quad (14)$$

$$\boldsymbol{v}_{ext} = \begin{bmatrix} v_x & v_y & v_z & \omega_x & \omega_y & \omega_z \end{bmatrix}^T = \begin{bmatrix} \boldsymbol{v} \\ \boldsymbol{\omega} \end{bmatrix} \quad (15)$$

and $\boldsymbol{v}_{int} \in \mathcal{R}^{n-6}$ is the vector of internal velocities (virtual in case of a rigid body) deforming the body.

3.2 Skill Example of Sliding Contact

The following example illustrates Proposition 1 with a simple manipulation example. Let us consider the pen shown in Fig. 6, grasped by four fingers, each acting on the pen by three wrenches (Coulomb friction model). The task is to

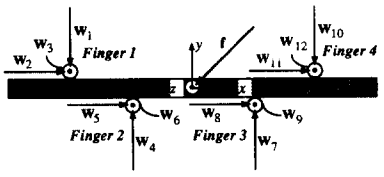

Figure 6: Pen Example Grasped by 4 Fingers.

move one finger after another to the left while sliding over the surface of the pen without breaking contact during four corresponding time intervals $t_{i-1} \leq t < t_i$. To realize this, internal grasping forces must be chosen appropriately.

In the following we write this task with sliding contact motions in terms of the matrix $\boldsymbol{W}(t)$ of (3) as

$$\boldsymbol{W} = \begin{bmatrix} 0 & 1 & 0 & 0 & 1 & 0 & 0 & 1 & 0 & 0 & 1 & 0 \\ -1 & 0 & 0 & 1 & 0 & 0 & 1 & 0 & 0 & -1 & 0 & 0 \\ 0 & 0 & 1 & 0 & 0 & 1 & 0 & 0 & 1 & 0 & 0 & 1 \\ 0 & 0 & r & 0 & 0 & -r & 0 & 0 & -r & 0 & 0 & r \\ 0 & 0 & \phi_1 & 0 & 0 & \phi_2 & 0 & 0 & -\phi_3 & 0 & 0 & -\phi_4 \\ \phi_1 & -r & 0 & -\phi_2 & r & 0 & \phi_3 & r & 0 & -\phi_4 & -r & 0 \end{bmatrix} \tag{16}$$

where

$$\phi_i(t) = \begin{cases} l_i & 0 \leq t < t_{i-1} \\ l_i + \alpha_i(t - t_{i-1}) & t_{i-1} \leq t < t_i \\ l_i + \alpha_i(t_i - t_{i-1}) & t_i \leq t \end{cases} \tag{17}$$

for $i = 1, .., 4$, and l_i denotes the initial distance of finger i from the center of mass, r is the radius of the pen and $\alpha_i \geq 0$, determines the sliding speed. The external disturbing force $\boldsymbol{f}_{ext}(t)$ is the constant gravitational force:

$$\boldsymbol{f}_{ext}(t) = \begin{bmatrix} 0 & -mg & 0 & 0 & 0 & 0 \end{bmatrix}^T \tag{18}$$

The internal grasp forces may be chosen arbitrarily within the limits of frictional constraints. In the above example of sliding contacts, we can write the following friction and contact constraints for the 4 steps of sliding contact motion, where Coulomb friction is linearized with a conservative estimation for the friction coefficient μ. The wrench intensities are denoted by c_i for wrench $\boldsymbol{w}_i$, $i = 1, .., 12$. For maintaining contacts we need the normal wrench intensities to be

$$c_i \geq f_0 \qquad i = 1, 4, 7, 10 \tag{19}$$

where f_0 is a minimal bias contact force. For sliding contact of finger i, the friction constraints for the three contact wrench intensities c_j, c_{j+1}, c_{j+2} of finger k follow as

$$c_{j+1} + \mu c_j < 0 \qquad k = i \tag{20}$$
$$c_{j+1} + \mu c_j \geq 0 \qquad k \neq i \tag{21}$$
$$c_{j+1} - \mu c_j \leq 0 \qquad k \neq i \tag{22}$$
$$c_{j+2} + \mu c_j \geq 0 \qquad k \neq i \tag{23}$$
$$c_{j+2} - \mu c_j \leq 0 \qquad k \neq i \tag{24}$$

where $j = 3k - 2$ and $k = 1, .., 4$. The magnitudes of the internal grasping forces can easily be found using the Simplex algorithm solving the above linear programming problems.

Having determined the dynamic behavior of $\boldsymbol{G}(t)$ and the reference trajectories for the contact wrench intensities $c_i(t)$, they can be realized using the control algorithm derived in the following section.

3.3 Control Algorithm Derivation

3.3.1 Control Problem

The desired body trajectory can be written in terms of world coordinates as

$$\boldsymbol{p}^d(t) = Trans(\boldsymbol{r}^d(t))\ RPY(\boldsymbol{\varphi}^d(t))\ , \tag{25}$$

where $\boldsymbol{r}$ designates the vector from the the coordinate origin to the center of mass of the body, and $RPY(\boldsymbol{\varphi})$ the roll-pitch-yaw orientation of the body coordinate frame, with $\boldsymbol{\varphi} = [\phi_1\ \phi_2\ \phi_3]^T$ the roll, pitch and yaw angles. Then the body velocity can be written in terms of $\boldsymbol{r}, \boldsymbol{\varphi}$ as

$$\begin{bmatrix} \boldsymbol{v} \\ \boldsymbol{\omega} \end{bmatrix} = \boldsymbol{\Psi}(\boldsymbol{r}, \boldsymbol{\varphi}) \begin{bmatrix} \dot{\boldsymbol{r}} \\ \dot{\boldsymbol{\varphi}} \end{bmatrix} . \tag{26}$$

Differention of Equation (26) leads to linear and angular acceleration of the body

$$\begin{bmatrix} \dot{\boldsymbol{v}} \\ \dot{\boldsymbol{\omega}} \end{bmatrix} = \boldsymbol{\Psi}(\boldsymbol{r}, \boldsymbol{\varphi}) \begin{bmatrix} \ddot{\boldsymbol{r}} \\ \ddot{\boldsymbol{\varphi}} \end{bmatrix} + \dot{\boldsymbol{\Psi}}(\boldsymbol{r}, \boldsymbol{\varphi}) \begin{bmatrix} \dot{\boldsymbol{r}} \\ \dot{\boldsymbol{\varphi}} \end{bmatrix} . \tag{27}$$

Also to maintain contact stability during manipulation the internal grasp force intensities must follow the given trajectory $\boldsymbol{c}_h^d(t)$. The object position error $\boldsymbol{e}_p(t) \in \mathcal{R}^6$ and the internal grasp force error $\boldsymbol{e}_f(t) \in \mathcal{R}^n$ are defined as

$$\boldsymbol{e}_p(t) = \begin{bmatrix} \boldsymbol{r}(t) \\ \boldsymbol{\varphi}(t) \end{bmatrix} - \begin{bmatrix} \boldsymbol{r}^d(t) \\ \boldsymbol{\varphi}^d(t) \end{bmatrix} \tag{28}$$

$$\boldsymbol{e}_f(t) = \boldsymbol{c}_h(t) - \boldsymbol{c}_h^d(t)\ . \tag{29}$$

The goal of the control algorithm is to assure both the object position error $\boldsymbol{e}_p(t)$ as well as the internal grasp force error $\boldsymbol{e}_f(t)$ to become zero.

3.3.2 Control Law

We can write the contact twist $\boldsymbol{d}$ as in Equation (8) as well as in terms of the hand Jacobian $\boldsymbol{J}(\boldsymbol{\theta})$

$$\boldsymbol{d} = \boldsymbol{G}^{-1}\ \boldsymbol{\mathcal{V}} = \boldsymbol{J}(\boldsymbol{\theta})\ \dot{\boldsymbol{\theta}}\ . \tag{30}$$

Differentiating Equation (30) with respect to time leads to

$$\boldsymbol{G}^{-1}\dot{\boldsymbol{\mathcal{V}}} + \dot{\boldsymbol{G}}^{-1}\boldsymbol{\mathcal{V}} = \boldsymbol{J}\ \ddot{\boldsymbol{\theta}} + \dot{\boldsymbol{J}}\ \dot{\boldsymbol{\theta}}\ . \tag{31}$$

Assuming that the grasp in fully manipulable, i.e. $\mathcal{R}(\boldsymbol{J}) \subset \mathcal{R}(\boldsymbol{G}^{-1})$ we can write the joint acceleration $\ddot{\boldsymbol{\theta}}$ as

$$\ddot{\boldsymbol{\theta}} = \boldsymbol{J}^+ \left[\boldsymbol{G}^{-1}\dot{\boldsymbol{\mathcal{V}}} + \dot{\boldsymbol{G}}^{-1}\boldsymbol{\mathcal{V}} - \dot{\boldsymbol{J}}\ \dot{\boldsymbol{\theta}}\right] , \tag{32}$$

where $\boldsymbol{J}^+ = \boldsymbol{J}^T(\boldsymbol{J}\boldsymbol{J}^T)^{-1}$ is the generalized inverse of $\boldsymbol{J}$.

The object dynamics are given by the Newton-Euler equations

$$\begin{bmatrix} \hat{\boldsymbol{m}} & \boldsymbol{0} \\ \boldsymbol{0} & \boldsymbol{\mathcal{J}} \end{bmatrix} \begin{bmatrix} \dot{\boldsymbol{v}} \\ \dot{\boldsymbol{\omega}} \end{bmatrix} + \begin{bmatrix} \boldsymbol{\omega} \times \hat{\boldsymbol{m}}\boldsymbol{v} \\ \boldsymbol{\omega} \times \boldsymbol{\mathcal{J}}\boldsymbol{\omega} \end{bmatrix} = \boldsymbol{f}_{ext}\ , \tag{33}$$

where $\hat{\boldsymbol{m}} \in \mathcal{R}^{3\times3}$ is a diagonal matrix with the object mass in the diagonal elements and $\boldsymbol{\mathcal{J}} \in \mathcal{R}^{3\times3}$ is the inertia tensor. The ith finger dynamic equation is found to be

$$\boldsymbol{M}_i(\boldsymbol{\theta}_i)\ \ddot{\boldsymbol{\theta}}_i + \boldsymbol{H}_i(\boldsymbol{\theta}_i, \dot{\boldsymbol{\theta}}_i) = \boldsymbol{\tau}_i$$
$$-\boldsymbol{J}_i^T(\boldsymbol{\theta}_i) \begin{bmatrix} \boldsymbol{w}_i^1 & \ldots & \boldsymbol{w}_i^j \end{bmatrix} \begin{bmatrix} c_i^1 \\ \vdots \\ c_i^j \end{bmatrix} . \tag{34}$$

where $i = 1, \ldots, k$, $j = 1, \ldots, n_i$, k =number of fingers, n_i = number of wrenches exerted by finger i. m_i = degrees of freedom of finger i, $\boldsymbol{M}_i(\boldsymbol{\theta}_i) \in \mathcal{R}^{m_i \times m_i}$ is the moment of inertia matrix, $\boldsymbol{H}_i(\boldsymbol{\theta}_i, \dot{\boldsymbol{\theta}}_i) \in \mathcal{R}^{m_i}$ includes centrifugal, Coriolis and gravitational forces. $\boldsymbol{\tau}_i \in \mathcal{R}^{m_i}$ is the vector of joint torques. $\boldsymbol{w}_i^j$ is the direction the wrench j of finger i is applied and c_i^j is the corresponding wrench intensity. All finger dynamic equations can be written into one matrix differential equation as

$$\boldsymbol{M}(\boldsymbol{\theta})\,\ddot{\boldsymbol{\theta}} + \boldsymbol{H}(\boldsymbol{\theta}, \dot{\boldsymbol{\theta}}) = \boldsymbol{\tau} - \boldsymbol{J}^T(\boldsymbol{\theta})\,\boldsymbol{c}\,. \tag{35}$$

where

$$\begin{aligned} \boldsymbol{M}(\boldsymbol{\theta}) &= \mathbf{diag}(\boldsymbol{M}_1(\boldsymbol{\theta}_1) \ldots \boldsymbol{M}_k(\boldsymbol{\theta}_k)) \\ \boldsymbol{J}(\boldsymbol{\theta}) &= \mathbf{diag}(\boldsymbol{J}_1(\boldsymbol{\theta}_1) \ldots \boldsymbol{J}_k(\boldsymbol{\theta}_k)) \\ \boldsymbol{H}(\boldsymbol{\theta}, \dot{\boldsymbol{\theta}}) &= [\boldsymbol{H}_1(\boldsymbol{\theta}_1, \dot{\boldsymbol{\theta}}_1) \ldots \boldsymbol{H}_k(\boldsymbol{\theta}_k, \dot{\boldsymbol{\theta}}_k)]^T \\ \boldsymbol{\tau} &= [\boldsymbol{\tau}_1 \ldots \boldsymbol{\tau}_k]^T\,. \end{aligned}$$

Substituting Equation (32), (33), using (11) into (35), and recalling the definition of $\boldsymbol{\mathcal{V}}$ in Equation (14) yields

$$\begin{aligned} \boldsymbol{M}\boldsymbol{J}^+ \left\{ \boldsymbol{W}^T \begin{bmatrix} \dot{\boldsymbol{v}} \\ \dot{\boldsymbol{\omega}} \end{bmatrix} + \dot{\boldsymbol{W}}^T \begin{bmatrix} \boldsymbol{v} \\ \boldsymbol{\omega} \end{bmatrix} + \boldsymbol{N}\dot{\boldsymbol{v}}_{int} + \dot{\boldsymbol{N}}\boldsymbol{v}_{int} - \dot{\boldsymbol{J}}\,\dot{\boldsymbol{\theta}} \right\} \\ + \boldsymbol{H}(\boldsymbol{\theta}, \dot{\boldsymbol{\theta}}) = \boldsymbol{\tau} - \boldsymbol{J}^T\boldsymbol{c}_h \\ -\boldsymbol{J}^T\boldsymbol{W}^+ \left\{ \begin{bmatrix} \hat{m} & \boldsymbol{0} \\ \boldsymbol{0} & \boldsymbol{\mathcal{J}} \end{bmatrix} \begin{bmatrix} \dot{\boldsymbol{v}} \\ \dot{\boldsymbol{\omega}} \end{bmatrix} + \begin{bmatrix} \boldsymbol{\omega} \times \hat{m}\boldsymbol{v} \\ \boldsymbol{\omega} \times \boldsymbol{\mathcal{J}}\boldsymbol{\omega} \end{bmatrix} \right\}\,. \end{aligned} \tag{36}$$

Let us define $\boldsymbol{\tau}$ to be the sum of $\boldsymbol{\tau}_1$ still to be determined and some terms for cancellation in Equation (36)

$$\begin{aligned} \boldsymbol{\tau} &= \boldsymbol{\tau}_1 + \boldsymbol{M}\boldsymbol{J}^+ \left\{ \dot{\boldsymbol{W}}^T \begin{bmatrix} \boldsymbol{v} \\ \boldsymbol{\omega} \end{bmatrix} + \boldsymbol{N}\dot{\boldsymbol{v}}_{int} + \dot{\boldsymbol{N}}\boldsymbol{v}_{int} - \dot{\boldsymbol{J}}\,\dot{\boldsymbol{\theta}} \right\} \\ &+ \boldsymbol{H}(\boldsymbol{\theta}, \dot{\boldsymbol{\theta}}) + \boldsymbol{J}^T\boldsymbol{W}^+ \begin{bmatrix} \boldsymbol{\omega} \times \hat{m}\boldsymbol{v} \\ \boldsymbol{\omega} \times \boldsymbol{\mathcal{J}}\boldsymbol{\omega} \end{bmatrix}\,. \end{aligned} \tag{37}$$

Substitution of Equation (37) into (36) yields

$$\boldsymbol{M}^* \begin{bmatrix} \dot{\boldsymbol{v}} \\ \dot{\boldsymbol{\omega}} \end{bmatrix} = \boldsymbol{\tau}_1 - \boldsymbol{J}^T\boldsymbol{c}_h\,, \tag{38}$$

where

$$\boldsymbol{M}^* = \boldsymbol{M}\boldsymbol{J}^+\boldsymbol{W}^T + \boldsymbol{J}^T\boldsymbol{W}^+ \begin{bmatrix} \hat{m} & \boldsymbol{0} \\ \boldsymbol{0} & \boldsymbol{\mathcal{J}} \end{bmatrix}. \tag{39}$$

Inserting Equation (27) into (38) yields

$$\boldsymbol{M}^* \left\{ \boldsymbol{\Psi}(\boldsymbol{r}, \boldsymbol{\varphi}) \begin{bmatrix} \ddot{\boldsymbol{r}} \\ \ddot{\boldsymbol{\varphi}} \end{bmatrix} + \dot{\boldsymbol{\Psi}}(\boldsymbol{r}, \boldsymbol{\varphi}) \begin{bmatrix} \dot{\boldsymbol{r}} \\ \dot{\boldsymbol{\varphi}} \end{bmatrix} \right\} = \boldsymbol{\tau}_1 - \boldsymbol{J}^T\boldsymbol{c}_h\,. \tag{40}$$

Defining $\boldsymbol{\tau}_1$ as

$$\begin{aligned} \boldsymbol{\tau}_1 &= \boldsymbol{M}^*\dot{\boldsymbol{\Psi}}(\boldsymbol{r}, \boldsymbol{\varphi}) \begin{bmatrix} \dot{\boldsymbol{r}} \\ \dot{\boldsymbol{\varphi}} \end{bmatrix} + \boldsymbol{J}^T \left[\boldsymbol{c}_h^d - \frac{1}{\delta}\dot{\boldsymbol{e}}_f - \frac{1}{\delta}\boldsymbol{W}^+\dot{\boldsymbol{W}}\boldsymbol{e}_f \right] \\ &+ \boldsymbol{M}^*\boldsymbol{\Psi}(\boldsymbol{r}, \boldsymbol{\varphi}) \left\{ \begin{bmatrix} \ddot{\boldsymbol{r}}^d \\ \ddot{\boldsymbol{\varphi}}^d \end{bmatrix} - \boldsymbol{K}_v\dot{\boldsymbol{e}}_p - \boldsymbol{K}_p\boldsymbol{e}_p \right\}. \end{aligned} \tag{41}$$

Inserting Equation (41) into (40) yields

$$\begin{aligned} \boldsymbol{M}^*\boldsymbol{\Psi}(\boldsymbol{r}, \boldsymbol{\varphi})\,[\ddot{\boldsymbol{e}}_p + \boldsymbol{K}_v\dot{\boldsymbol{e}}_p + \boldsymbol{K}_p\boldsymbol{e}_p] = \\ -\boldsymbol{J}^T \left[\boldsymbol{e}_f + \frac{1}{\delta}\dot{\boldsymbol{e}}_f + \frac{1}{\delta}\boldsymbol{W}^+\dot{\boldsymbol{W}}\boldsymbol{e}_f \right]. \end{aligned} \tag{42}$$

Given the positive definiteness of $\boldsymbol{M}^*$ we can always find appropriate gain matrices $\boldsymbol{K}_v, \boldsymbol{K}_p$ to make

$$\ddot{\boldsymbol{e}}_p + \boldsymbol{K}_v\dot{\boldsymbol{e}}_p + \boldsymbol{K}_p\boldsymbol{e}_p = 0\,, \tag{43}$$

which shows that the position error $\boldsymbol{e}_p$ can be made zero. Now substituting Equation (43) into (42) and assuming that $\boldsymbol{J}$ is of full rank, we then get the following first order differential equation for the force error $\boldsymbol{e}_f$

$$\dot{\boldsymbol{e}}_f = -(\delta\boldsymbol{I} + \boldsymbol{W}^+\dot{\boldsymbol{W}})\boldsymbol{e}_f\,. \tag{44}$$

Equation (44) can be made asymptotically stable by choosing a sufficiently large δ and therewith making all eigenvalues of $-(\delta\boldsymbol{I} + \boldsymbol{W}^+\dot{\boldsymbol{W}})$ negative.

We can now summarize the derived control law in the following Theorem.

Theorem 1 *The position trajectory error $\boldsymbol{e}_p$ defined in Equation (28) and the internal grasp force error $\boldsymbol{e}_f$ defined in Equation (29) can be made zero by the control law as*

$$\begin{aligned} \boldsymbol{\tau} &= \boldsymbol{M}^*\dot{\boldsymbol{\Psi}}(\boldsymbol{r}, \boldsymbol{\varphi}) \begin{bmatrix} \dot{\boldsymbol{r}} \\ \dot{\boldsymbol{\varphi}} \end{bmatrix} + \boldsymbol{H}(\boldsymbol{\theta}, \dot{\boldsymbol{\theta}}) \\ &+ \boldsymbol{M}^*\boldsymbol{\Psi}(\boldsymbol{r}, \boldsymbol{\varphi}) \left\{ \begin{bmatrix} \ddot{\boldsymbol{r}}^d \\ \ddot{\boldsymbol{\varphi}}^d \end{bmatrix} - \boldsymbol{K}_v\dot{\boldsymbol{e}}_p - \boldsymbol{K}_p\boldsymbol{e}_p \right\} \\ &+ \boldsymbol{J}^T \left\{ \boldsymbol{c}_h^d - \frac{1}{\delta}\dot{\boldsymbol{e}}_f - \frac{1}{\delta}\boldsymbol{W}^+\dot{\boldsymbol{W}}\boldsymbol{e}_f + \boldsymbol{W}^+ \begin{bmatrix} \boldsymbol{\omega} \times \hat{m}\boldsymbol{v} \\ \boldsymbol{\omega} \times \boldsymbol{\mathcal{J}}\boldsymbol{\omega} \end{bmatrix} \right\} \\ &+ \boldsymbol{M}\boldsymbol{J}^+ \left\{ \dot{\boldsymbol{W}}^T \begin{bmatrix} \boldsymbol{v} \\ \boldsymbol{\omega} \end{bmatrix} + \boldsymbol{N}\dot{\boldsymbol{v}}_{int} + \dot{\boldsymbol{N}}\boldsymbol{v}_{int} - \dot{\boldsymbol{J}}\,\dot{\boldsymbol{\theta}} \right\}. \end{aligned} \tag{45}$$

where $\boldsymbol{M}^*$ is defined in Equation (39) and $\delta > 0$ is sufficiently large to make the force error $\boldsymbol{e}_f(t)$ defined in Equation (29) governed by the differential equation (44) become zero.

4 Experiments and Simulations

4.1 Calibration Result

If one tries to form the angle vector Θ of the index finger of the hand model in the virtual world simulator using variable scheduled gains for linearly combining the sensor angles ψ_i, $i = 1, 2$, calibration cannot be achieved. Even tuning the gain parameters to optimal values will lead to a false hand position as shown in Fig. 7(a), if the human operator's thumb and index finger are in contact. Figure 7(b) shows the same hand position after mapping $\Theta = f(\Psi)$ using the trained ANN described in section 2.4. It is obvious that the proposed method of learning the nonlinear mapping by an ANN is very effective.

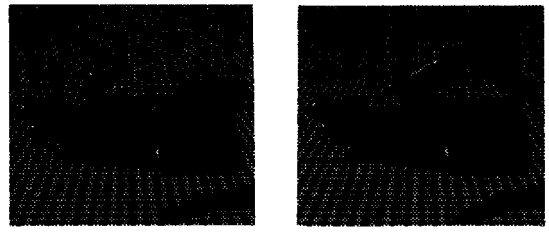

(a) Linear combination (b) Using the trained ANN

Figure 7: Calibration Result.

4.2 Grasp Wrench Trajectory Calculation of Skill Example

Assuming the example skill described in section 3.2 and the following parameters: Coulomb friction coefficient $\mu =$

0.25, pen radius $r = 1\ cm$, length $l = 10\ cm$, mass $mg = 1\ N$, finger initial distances from center of mass and sliding speed parameters $l_1 = 3\ cm$, $l_2 = 2\ cm$, $l_3 = 2\ cm$, $l_4 = 3\ cm$, $\alpha_i = 1\ cm\ sec^{-1}$, time intervals $t_0 = 0\ sec$, $t_1 = 1\ sec$, $t_2 = 2\ sec$, $t_3 = 3\ sec$, $t_4 = 4\ sec$. Figure 8 shows the reference trajectories for the wrench intensities, where the following do not vary with time: $c_1 = 0.1\ N$, $c_2 = -0.025\ N$, $c_3 = -0.025\ N$, $c_6 = 0.04\ N$, $c_9 = -0.04\ N$, $c_{10} = 0.1\ N$, $c_{11} = -0.025\ N$, $c_{12} = 0.025\ N$.

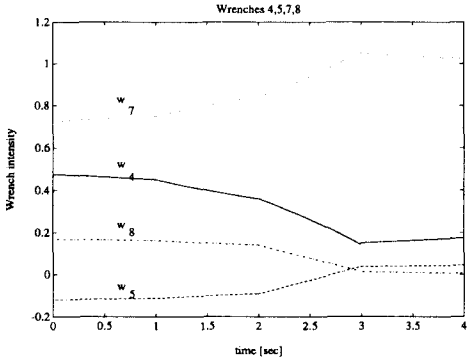

Figure 8: Wrench Intensities for Skill Example.

4.3 Simulation of Control Algorithm

Let us again assume the skill example of the pen grasped by 4 fingers (see Fig. 6) and rotate the pen around the z-axis. The control goal according to section 3.3 is then to control the pen position to rest $\boldsymbol{r}^d(t) = [0\ 0\ 0]^T$ and the RPY-angles to rotate around the z-axis $\boldsymbol{\varphi}^d(t) = [\sin\omega t\ 0\ 0]^T$, where ω is the angular velocity of rotation. Figure 9 shows that the initial angular position error decreases to zero asymptotically.

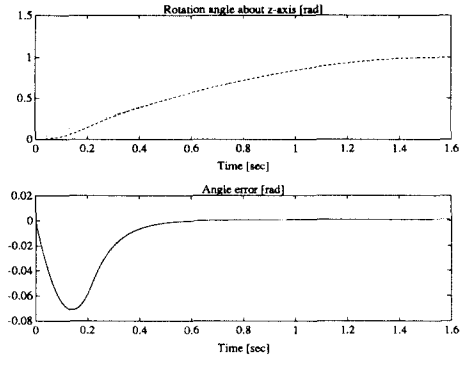

Figure 9: Simulation of Pen Rotation.

5 Conclusion

We have proposed the idea of an *Intelligent Assisting System — IAS*. Ongoing research will lead to an understanding of human manipulative skill with the goal to create a manipulation skill data base. Using this data base the IAS is able to perform very complex manipulation tasks on the motion control level forming an intelligent assistant to a human operator. In particular we described the following

- Definition of the IAS and its functional modules.
- Sensor glove with 10 degrees-of-freedom for interaction of the human operator with objects of a virtual world.
- Calibration method for this sensor glove using an artificial neural network to learn and approximate the nonlinear calibration function.
- A model for manipulative skill based on the grip transformation matrix.
- A control algorithm in hand joint space to realize the acquired manipulation skill.

Experimental results confirmed the good efficiency of the proposed calibration method using an artificial neural network. A simple example indicated that the proposed model is useful to describe manipulative skill and the efficiency of the control law.

Acknowledgements

The authors would like to thank Mr. Koji Mukai for his extraordinary support during the development of the sensor glove experimental system and Prof. Fumio Harashima for many valuable discussions and his constant encouragement.

This research was partly supported by the Electro-Mechanic Technology Advancing Foundation.

References

[1] Cole, A., Hsu, P., Sastry, S.S., 1992. Dynamic Control of Sliding by Robot Hands for Regrasping. *Transactions on Robotics and Automation*, Vol.8, No.1, February 1992, pp.42-52.

[2] Hashimoto, H., Buss, M., Skill Acquisition for the Intelligent Assisting System Using Virtual Reality Simulator, The 2nd International Conference on Artificial Reality and Tele-Existance ICAT'92, pp.37-46, 1992.

[3] Hashimoto, H., Buss, M., Analysis and Synthesis of Human Skill for Intelligent Assisting System, *IEEE International Workshop on Robot and Human Communication ROMAN'92*, 1992.

[4] Iwata, H., 1990. Artificial Reality with Force-feedback: Development of Desktop Virtual Space with Compact Master Manipulator. *Computer Graphics*, Vol.24, No.4, pp.59-64.

[5] Kerr, J. and Roth, B., 1986. Analysis of Multifingered Hands. *Int. J. of Robotics Research*, Vol.4, No.4, 1986, pp.3-17.

[6] Kobayashi, H., 1985. Control and Geometrical Considerations for an Articulated Robot Hand. *Int. J. of Robotics Research*, Vol.4, No.1, Spring 1985, pp.3-12.

[7] Li, Z., Sastry, S.S., 1988. Task-Oriented Optimal Grasping by Multifingered Robot Hands. *Journal of Robotics and Automation*, Vol.4, No.1, February 1988, pp.32-44.

[8] Mason, M.T., Salisbury, J.K., 1985. Robot Hands and the Mechanics of Manipulation. *MIT Press*, Cambridge, Massachusetts, 1985.

[9] Salisbury, J.K. and Craig, J.J., 1982. Articulated Hands: Force Control and Kinematic Issues. *Int. J. of Robotics Research*, Vol.1, No.1, Spring 1982, pp.4-17.